Applied Soft Computing Journal 89 (2020) 106126

Contents lists available at ScienceDirect

Applied Soft Computing Journal

journal homepage: www.elsevier.com/locate/asoc

Reconstruction method with the learned regularizer for imaging problems in electrical capacitance tomography

J. Lei [a,*], Q.B. Liu [b]

[a] School of Energy, Power and Mechanical Engineering, North China Electric Power University, Changping District, Beijing 102206, China
[b] Institute of Engineering Thermophysics, Chinese Academy of Sciences, Haidian District, Beijing 100190, China

ARTICLE INFO

Article history:
Received 1 November 2018
Received in revised form 27 June 2019
Accepted 21 January 2020
Available online 28 January 2020

Keywords:
Image reconstruction
Least square support vector machine
Random projection
Ensemble learning
Learned regularization
Regularized imaging method
Differential evolution algorithm
Inverse problem
Electrical capacitance tomography

ABSTRACT

The electrical capacitance tomography (ECT) is an attractive tomography method for process monitoring applications across different tasks and domains, but low quality images deteriorate its reliability and applicability. In order to change this situation, a potent method is developed to reduce reconstruction artifacts in this study. The learned regularization (LR) from a new ensemble learning method that integrates the advantageous properties of the least square support vector machine (LSSVM) method, the random projection (RP) method and the sparse matrix regression (SMR) solved by the differential evolution (DE) algorithm is proposed to increase the elasticity in mining and utilizing the prior knowledge. A potent model for imaging is devised by simultaneously taking advantage of the domain knowledge of the reconstruction targets (RTs) and the LR. The iterative split Bregman (ISB) is extended into a simple but powerful solver for the devised model by leveraging the forward backward splitting (FBS) algorithm and the soft thresholding (ST) algorithm to solve sub-problems efficiently. The imaging method proposed in the study is validated to successfully work on a series of testing tasks with the significant improvement of the reconstruction quality (RQ) over the popular imaging methods.

1. Introduction

As a non-contacting monitoring modality, the ECT is an attractive method for non-destructively recovering the distribution of permittivity and hence the distribution of material by solving an ill-posed problem. The technique, with the comparative superiorities of fast response, non-radiation, good portability and non-contacting measurement, is impacting a wide range of process monitoring applications across different tasks and domains. For instance, the technology has been applied to monitor time-varying behaviors of materials in oil pipelines, pharmaceutical manufacturing process, frozen soil engineering, circulating fluidized beds and cyclone separators.

The applicability of the technology is challenged by low-quality images that significantly lower the reliability and usefulness of measurement results. The quality of recovered images is greatly impacted by the numerical properties of a solver. Concretely, a suited numerical solver potentially reduces reconstruction artifacts and weakens deformations. On the contrary, an unsuitable solver very likely produces unreasonable images, deteriorating the reliability and usefulness of results. Many pioneers try to weaken reconstruction deformations and reduce reconstruction artifacts by leveraging the superiorities of numerical algorithm. A considerable amount of literatures has been published for fulfilling this goal, and a list about the published articles is summarized in [1–27]. In these published methods, we can divide them into two types (non-iterative solvers [1–4] and iterative solvers [5–27]). The non-iterative solvers commonly yield unreasonable images in spite of fulfilling fast reconstruction. To change this dilemma, researchers devote to devising more powerful iterative solver. The iteration Landweber (IL) algorithm is a well-known and prevalent solver in handling inverse problems [5]. Martin et al. [6] developed an iterative regularization method. In [8–10], the sparseness regularization method has been introduced for imaging. The ISB algorithm has been employed by Hosani et al. [11]. The paper [13] provided the level set technique. Xia et al. [14] tailored the alternating direction method of multipliers (ADMM) for reconstruction tasks. Instead of employing a deterministic optimization algorithm, Wang et al. [15] introduced a stochastic optimization method for reconstruction, in which the capacitance errors were forecasted by the LSSVM method. Zhang et al. [16] developed a wavelet fusion-based reconstruction approach. Taking the place of using the L_2 norm as a regularizer, the papers [17–19] devised the cost functions with the total variation (TV) as a regularizer. The potent solvers have been developed for handling time-varying RTs [20,21]. Cao et al. [23] proposed an iterative solver based on the Calderon's method. Recently, Chu et al. [24] reported an imaging technique

* Corresponding author.
E-mail address: leijing2002@126.com (J. Lei).

https://doi.org/10.1016/j.asoc.2020.106126
1568-4946/

Nomenclature

Abbreviations

ADMM	Alternating direction method of multipliers
ART	Algebraic reconstruction technique
CIP	Cimmino iterative projection
CR	Combination regularization
DE	Differential evolution
ECT	Electrical capacitance tomography
ELSSVM	Ensemble least square support vector machine
FBS	Forward backward splitting
FR	Fractional regularization
FRCG	Fletcher–Reeves conjugate gradient
IE	Image error
ISB	Iterative split Bregman
IL	Iteration Landweber
LBP	Linear back projection
LoN	Level of noise
LR	Learned regularization
L1R	L_1 regularization
L2R	L_2 regularization
LRR	Learned regularization reconstruction
LSSVM	Least square support vector machine
NoI	Numbers of iterations
OIOR	Offline iteration online reconstruction
RP	Random projection
RT	Reconstruction target
RQ	Reconstruction quality
SKI	Sparse Kaczmarz iteration
SMR	Sparse matrix regression
SS	Step size
ST	Soft thresholding
TVR	Total variation regularization
TSVD	Truncated singular value decomposition

Symbols

$\boldsymbol{A}$	Sensitivity matrix
$\boldsymbol{b}$	Variable
$c1$, $c2$ and $c3$	Integral number
$\boldsymbol{d}$	Variable
$\boldsymbol{D}$	Difference matrix
$\boldsymbol{e}$	Error variable
f	Function
F	Function
g	Variable
h	Variable
$\boldsymbol{H}$	Base image matrix
l	Variable
$\boldsymbol{K}$	Kernel matrix
$\boldsymbol{I}$	Identity matrix
q	Variable
$\boldsymbol{R}$	Variable
$\boldsymbol{r}$, $\boldsymbol{s}$	Variable
$\boldsymbol{S}$	Data matrix
$\boldsymbol{u}$	Variable
$\boldsymbol{z}$	Variable

Greek symbols

$\boldsymbol{\rho}$	Lagrange multiplier
η	Regularization parameter
σ, τ	Kernel parameter
$\boldsymbol{\psi}$	Projection matrix
$\boldsymbol{\varepsilon}$, ζ, μ, β, $\boldsymbol{o}$	Variable
$\boldsymbol{\theta}$	Coefficient vector
$\boldsymbol{\omega}$	Weight vector
λ	Regularization parameter
φ	Function
$\boldsymbol{\Xi}$	Weight matrix
ς	Thresholding value

using priors from the convolutional extreme learning machine, in which the devised cost function was solved by the ADMM. Instead of taking advantage of a single regularizer, Guo et al. [25] and Tong at el. [26] have developed combination regularization (CR) methods to further reduce reconstruction artifacts. To fulfill imaging tasks, Wang et al. [27] used the LSSVM method to extract the nonlinear mapping from measured capacitances to images. Lei et al. [28] reported an imaging approach based on the robust principle component analysis theory, and the alternating optimization method with the FBS method as a sub-problem solver was developed to solve the proposed cost function. Wang [18] and Yang and Peng [29] provided an overview on traditional numerical solvers for imaging. Researches show that the iterative regularization algorithm is the most dominant at the current stage.

The progress in imaging methods benefits mainly from the regularization theory about sparseness. The L_1 regularization (L1R) method has become very prevalent, bringing significant decrease in reconstruction artifacts beyond the L_2 regularization (L2R) technique. There are many available methods to handle the L1R problem. For instance, the ISB algorithm [30], the ADMM [31–33], the FBS algorithm [34,35], the DE technique with a local search approach [36], the neural network-based method [37,38], and refer to [39–43] for other popular solvers.

The above algorithms produce different behaviors with regard to different types of imaging tasks, and further improvement is still needed. Most of iterative solvers are derived from the solution process of an optimization problem formulating the imaging problem, and thus devising a suitable cost function is crucial. Different priors have been introduced into an imaging model, for instance, low rank, sparseness, and more. However, these priors still lead to unreasonable results, and it is necessary to mine and leverage other more effective image priors to reduce reconstruction artifacts. The ensemble learning is one of poplar machine learning methods. In the method, the forecasting quality of a single learner can be increased by simultaneously training several learners and combining their prediction results. The ensemble learning method has been deployed to a wide range of applications across different tasks and domains, but investigations on the computing imaging field are still scarce. To fulfill the gap, this study puts forward a new ensemble learning method to increase the forecasting quality of a prior image, and then a new regularizer, i.e., the LR, is devised with the prior image. The proposed ensemble learning method takes advantage of the superiorities of the LSSVM method served as a supervised base

learner, the RP method that is used to construct an ensemble of features to improve the diversity of ensemble and the SMR served as an aggregation method of solution ensemble. The DE algorithm without the requirement of the differentiability of an objective function is tailored to solve the devised SMR model. Further, the sparse prior and the LR are combined with a data fidelity term to yield a potent mathematical model for imaging.

It is an interesting topic to develop a powerful solver for an established cost function. Currently, the ADMM and the ISB technique have become popular solvers for optimization problems from image processing tasks. To fulfill the goal of reducing the expensive computation, however, we extend the ISB method into a simple but powerful hybrid solver by using the FBS algorithm and the ST method to solve sub-problems in this study.

To decrease reconstruction artifacts, the LR from a new ensemble learning method is devised, and a new regularization reconstruction model with a potent numerical solver is developed in this study. The research contributions are outlined as follows:

(1) The LR from a new ensemble learning method is put forward in this study, and a potent optimization model for imaging is devised by simultaneously taking advantage of the LR and the domain knowledge. The developed imaging model provides a new way towards mining and utilizing image priors, and brings a significant reduction in reconstruction artifacts.

(2) In order to reduce the expensive computation, in this work the ISB algorithm is extended into a potent hybrid solver for the developed reconstruction model by leveraging the ST algorithm and the FBS method to solve sub-problems efficiently.

(3) A new ensemble learning method that takes advantage of the superiorities of the LSSVM method, the RP technique and the SMR is developed to increase the prediction quality of a prior image. Concretely, the RP technique is deployed to capture an ensemble of data feature via setting different dimensionalities of feature and improve diversity, the LSSVM method is used as a supervised learner to obtain an ensemble of predictions, and the ensemble of solutions from the LSSVM method are fed into the SMR model that emphasizes the sparsity of the regression coefficients to yield a final prior image. The DE method, without the requirement of the differentiability of the cost function, is used as a powerful solver for the devised SMR model.

(4) Validation experiments verify that the developed imaging method outperforms over other popular algorithms, reduces reconstruction artifacts and weaken reconstruction deformations.

There are six sections in the rest of this article. Section 2 devises a new optimization model for imaging. A potent solver for the devised optimization model is developed in Section 3. Section 4 details the developed ELSSVM method. In Section 5, we specify the computing steps of the developed solver and clarify its favorable properties. Section 6 carries out numerical validations, which is followed by main research conclusions in Section 7.

2. Reconstruction model

Our presentation starts with discussing the imaging fundamentals, and then a new optimization model capitalizing on the learned prior image and the prior about sparseness is presented.

2.1. Common model in imaging

Following the physical principles behind reconstruction or imaging, recovering the high-dimensional permittivity distribution from its degraded low-dimensional capacitance measurement, the computing imaging problem of the ECT becomes [29], i.e.,

$$\boldsymbol{A}\boldsymbol{g} = \boldsymbol{y} + \boldsymbol{e} \tag{1}$$

where the matrix $\boldsymbol{A}$ gives a sensitivity map for each electrode pair, formulating the response of the physically measurement device; $\boldsymbol{g}$ means the unknown permittivity distribution vector; the capacitance measurement vector with a lower dimensionality than the permittivity distribution vector and the noise vector are defined by $\boldsymbol{y}$ and $\boldsymbol{e}$, respectively.

To weaken the ill-pose nature while reducing reconstruction artifacts, the regularization technique is a promising alternative, which aims at minimizing a general cost function of the form:

$$\min\left\{f(\boldsymbol{g},\boldsymbol{y}) + \sum_{j=1}^{n}\lambda_j\varphi_j(\boldsymbol{g})\right\} \tag{2}$$

where $f(\boldsymbol{g},\boldsymbol{y})$ measures the data fidelity that favors the consistence between solutions and measurements; $\varphi_j(\boldsymbol{g})$ represents a regularizer that allows desired properties about the latent variables to be solved and $\lambda_j > 0$ adjusts the intensity of regularization. Eq. (2) is a universal cost function and can be extended into different forms.

The L2R method aims at minimizing the following loss function of the form:

$$\min\left\{\|\boldsymbol{A}\boldsymbol{g} - \boldsymbol{y}\|^2 + \lambda\|\boldsymbol{g}\|^2\right\} \tag{3}$$

Unlike the L2R technique, the fractional regularization method solves the following optimization problem [44,45]:

$$\min\left\{\|\boldsymbol{A}\boldsymbol{g} - \boldsymbol{y}\|_{\boldsymbol{\Xi}}^2 + \lambda\|\boldsymbol{g}\|^2\right\} \tag{4}$$

where $\|\boldsymbol{g}\|_{\boldsymbol{\Xi}} = (\boldsymbol{g}^T\boldsymbol{\Xi}\boldsymbol{g})^{1/2}$, and $\boldsymbol{\Xi}$ is defined by $\boldsymbol{\Xi}=(\boldsymbol{A}\boldsymbol{A}^T)^{(\alpha-1)/2}$ with $\alpha > 0$.

In the TVR method, the following cost function needs to be solved:

$$\min\left\{\frac{1}{2}\|\boldsymbol{A}\boldsymbol{g} - \boldsymbol{y}\|^2 + \lambda\|\boldsymbol{g}\|_{\mathrm{TV}}\right\} \tag{5}$$

where $\|\cdot\|_{\mathrm{TV}}$ means the TV norm. Eq. (5) has no closed-form solution.

The L1R method enjoys the most prevalent sparseness regularization method, i.e.,

$$\min\left\{\frac{1}{2}\|\boldsymbol{A}\boldsymbol{g} - \boldsymbol{y}\|^2 + \lambda\|\boldsymbol{g}\|_1\right\} \tag{6}$$

where $\|\cdot\|_1$ defines the L_1 norm. There is no closed-form solution to Eq. (6).

2.2. Developed imaging model

To apply Eq. (2) to an actual problem, the functions, $f(\boldsymbol{g},\boldsymbol{y})$ and $\varphi_j(\boldsymbol{g})$, need to be established in advance. To simplify the recovery procedure, it is interesting to use a typical least squares fidelity term:

$$f(\boldsymbol{g},\boldsymbol{y}) = \frac{1}{2}\|\boldsymbol{A}\boldsymbol{g} - \boldsymbol{y}\|^2 \tag{7}$$

To promote a latent solution to satisfy the prior assumptions, devising a suited regularizer is very significant. Traditional methods cast the prior feature of an image into a penalty function, for example, low rank, sparsity, and more, which is further leveraged to design an imaging model. Dominant regularizers about sparseness include the L_0 norm, the L_1 norm, the $L_{1/2}$ norm, and others. In recent years, the L_1 norm-based sparseness regularizer has become very prevalent, producing impressive solutions. When it is deployed to the imaging problem in the ECT, unfortunately, the L1R commonly leads to unreasonable images. To fulfill the goal of enhancing the elasticity of regularization, researchers have put forward the CR, for example, $\|\boldsymbol{g}\|^2 + \|\boldsymbol{g}\|_1$, $\|\boldsymbol{G}\|_* + \|\boldsymbol{g}\|_1$, where $\boldsymbol{G}$ means a matrix generated by rearranging a vector $\boldsymbol{g}$

and $\|\cdot\|_*$ represents the nuclear norm, etc., to take advantage of much more priors. Plagued by the inherent limitations in these analytical priors, the CR still faces serious challenges in reducing reconstruction artifacts. To fulfill the goal of increasing the elasticity of a regularizer, we introduce the LR in the work, which is integrated with an analytical prior to yield a novel hybrid regularization for decreasing reconstruction artifacts. The hybrid regularization is composed of a LR and an analytical regularizer, which makes full use of the advantageous benefits of the both kinds of regularizers.

The TV norm is a widely-used regularizer. This work casts a prior image predicted by the proposed ELSSVM method into a LR by the TV norm:

$$\varphi_1(\boldsymbol{g}) = \|\boldsymbol{g} - \boldsymbol{g}_\ell\|_{\mathrm{TV}} \tag{8}$$

where $\boldsymbol{g}_\ell$ means a learned prior image from the proposed ELSSVM method. To reduce the expensive computation, the TV norm can be approximated by:

$$\varphi_1(\boldsymbol{g}) \approx \|\boldsymbol{D}(\boldsymbol{g} - \boldsymbol{g}_\ell)\|_1 \tag{9}$$

where $\boldsymbol{D} = [\boldsymbol{D}_x, \boldsymbol{D}_y]^T$, $\boldsymbol{D}_x$ and $\boldsymbol{D}_y$ are difference matrices.

The prior about sparseness has led to the boost in the spatial resolution, and this work also makes use of the prior, which is abstracted as follows:

$$\varphi_2(\boldsymbol{g}) = \sum_{i=1}^{N} \boldsymbol{w}_i|\boldsymbol{g}_i| \tag{10}$$

where $\boldsymbol{w}_i > 0$ is a problem-dependent weight vector. The introduction of the weighted vector leads to the enhancement in the elasticity of the regularizer. Obviously, Eq. (10) degrades into the standard L_1 norm with $\boldsymbol{w}_i = 1$.

Finally, the following minimization model can be obtained by submitting Eqs. (9) and (10) to Eq. (2):

$$\min\left\{\frac{1}{2}\|\boldsymbol{A}\boldsymbol{g} - \boldsymbol{y}\|^2 + \lambda_1\|\boldsymbol{D}(\boldsymbol{g} - \boldsymbol{g}_\ell)\|_1 + \lambda_2\sum_{i=1}^{N}\boldsymbol{w}_i|\boldsymbol{g}_i|\right\} \tag{11}$$

Two advantageous properties distinguish the developed model, Eq. (11), from conventional models for reconstruction. First, the LR and the prior about sparseness are simultaneously utilized, which opens a new approach towards mining image priors. Second, the developed model fulfills two goals, i.e., to incorporate relevant image priors and to stabilize computation process.

3. Numerical method

The intractable difficulty in solving Eq. (11) is derived from the inclusion of two non-smooth regularizers. One of possible selections is to employ a stochastic optimization algorithm without the differentiability of the cost function, such as the particle swarm optimization method [46], the genetic algorithm [47], the DE algorithm [48], the artificial bee colony optimization [49], the gray wolf optimization algorithm [50], etc., but it is challenging for these methods to solve problems with the large volume of unknown variables. To alleviate the challenges in calculation, the ISB method is extended to handle the devised cost function in this study, in which the ST algorithm and the FBS method are leveraged to solve sub-problems for lowering the costly computation.

It is convenient to rewrite Eq. (11) into a minimization problem of the form:

$$\begin{cases}\min\left\{\frac{1}{2}\|\boldsymbol{A}\boldsymbol{g} - \boldsymbol{y}\|^2 + \lambda_1\|\boldsymbol{d}\|_1 + \lambda_2\sum_{i=1}^{N}\boldsymbol{w}_i|\boldsymbol{g}_i|\right\} \\ s.t.\ \boldsymbol{d} = \boldsymbol{D}(\boldsymbol{g} - \boldsymbol{g}_\ell)\end{cases} \tag{12}$$

Following the basic principles behind the ISB method, the solution of Eq. (12) means solving the optimization problem below:

$$(\boldsymbol{d}^{k+1}, \boldsymbol{g}^{k+1}) = \min\left\{\frac{1}{2}\|\boldsymbol{A}\boldsymbol{g} - \boldsymbol{y}\|^2 + \lambda_1\|\boldsymbol{d}\|_1 + \lambda_2\sum_{i=1}^{N}\boldsymbol{w}_i|\boldsymbol{g}_i| + \frac{\beta}{2}\|\boldsymbol{d} - \boldsymbol{D}(\boldsymbol{g} - \boldsymbol{g}_\ell) - \boldsymbol{b}^k\|^2\right\} \tag{13}$$

The updating rule of the variable $\boldsymbol{b}$ has the following form:

$$\boldsymbol{b}^{k+1} = \boldsymbol{b}^k - (\boldsymbol{d}^{k+1} - \boldsymbol{D}(\boldsymbol{g}^{k+1} - \boldsymbol{g}_\ell)) \tag{14}$$

It is an intractable task to directly solve Eq. (13). To simplify computation, the problem is decoupled into the following more straightforward sub-problems by the alternating optimization method:

$$\boldsymbol{d}^{k+1} = \min\left\{\lambda_1\|\boldsymbol{d}\|_1 + \frac{\beta}{2}\|\boldsymbol{d} - \boldsymbol{D}(\boldsymbol{g}^k - \boldsymbol{g}_\ell) - \boldsymbol{b}^k\|^2\right\} \tag{15}$$

$$\boldsymbol{g}^{k+1} = \min\left\{\frac{1}{2}\|\boldsymbol{A}\boldsymbol{g} - \boldsymbol{y}\|^2 + \lambda_2\sum_{i=1}^{N}\boldsymbol{w}_i|\boldsymbol{g}_i| + \frac{\beta}{2}\|\boldsymbol{d}^{k+1} - \boldsymbol{D}(\boldsymbol{g} - \boldsymbol{g}_\ell) - \boldsymbol{b}^k\|^2\right\} \tag{16}$$

For Eq. (15), there is a closed-form solution, and it can be specified as:

$$\begin{aligned}\boldsymbol{d}^{k+1} &= \min\left\{\lambda_1\|\boldsymbol{d}\|_1 + \frac{\beta}{2}\|\boldsymbol{d} - \boldsymbol{D}(\boldsymbol{g}^k - \boldsymbol{g}_\ell) - \boldsymbol{b}^k\|^2\right\} \\ &= \mathrm{shrinkage}(\boldsymbol{D}(\boldsymbol{g}^k - \boldsymbol{g}_\ell) + \boldsymbol{b}^k, \lambda_1/\beta)\end{aligned} \tag{17}$$

where $\mathrm{shrinkage}(\cdot, \varsigma) = \max\{|\cdot| - \varsigma, 0\}\mathrm{sgn}(\cdot)$ is called the ST method, and $\mathrm{sgn}(\cdot)$ stands for a sign function.

It is interesting to find an efficient method to solve Eq. (16). The remarkable advantages of low computation complexity and high computing efficiency have made the FBS algorithm popular. Inherently, the FBS technique aims at solving the following optimization problem [34,35,51–53]:

$$\min\{H(\boldsymbol{g}) + \mu F(\boldsymbol{g})\} \tag{18}$$

where F and H define known problem-dependent functions.

The updating rule of the variable $\boldsymbol{g}$ in the FBS solver has the following form:

$$\boldsymbol{g}^{k+1} = \mathrm{Prox}_{\xi\mu F}(\boldsymbol{g}^k - \xi\,\partial H(\boldsymbol{g}^k)) \tag{19}$$

where $\mathrm{Prox}_{\xi\mu F}(\cdot)$ is given by:

$$\mathrm{Prox}_{\xi\mu F}(\boldsymbol{v}) = \min_{\boldsymbol{x}}\left\{\mu F(\boldsymbol{g}) + \|\boldsymbol{g} - \boldsymbol{v}\|^2/2\xi\right\} \tag{20}$$

In our case of $H(\boldsymbol{g}) = \|\boldsymbol{A}\boldsymbol{g} - \boldsymbol{y}\|^2/2 + \beta\|\boldsymbol{d}^{k+1} - \boldsymbol{D}(\boldsymbol{g} - \boldsymbol{g}_\ell) - \boldsymbol{b}^k\|^2/2$, it is easy to specify $\partial H(\boldsymbol{g}) = \boldsymbol{A}^T(\boldsymbol{A}\boldsymbol{g} - \boldsymbol{y}) + \beta\boldsymbol{D}^T(\boldsymbol{D}\boldsymbol{g} - \boldsymbol{D}\boldsymbol{g}_\ell + \boldsymbol{b}^k - \boldsymbol{d}^{k+1})$.

In Algorithm 1, the FBS-based computation method for solving Eq. (16) is outlined.

Algorithm 1: FBS-based computation method for solving equation (16)

1. The parameters for running the algorithm are given.

2. For $k = 0,1,2,\cdots$, implement the following iterative loop

Step 1. $\boldsymbol{v}^{k+1} = \boldsymbol{g}^k - \xi(\boldsymbol{A}^T(\boldsymbol{A}\boldsymbol{g}^k - \boldsymbol{y}) + \beta\boldsymbol{D}^T(\boldsymbol{D}\boldsymbol{g}^k - \boldsymbol{D}\boldsymbol{g}_\ell + \boldsymbol{b}^k - \boldsymbol{d}^{k+1}))$.

Step 2. $\boldsymbol{g}^{k+1} = \min_{\boldsymbol{x}}\left\{\lambda_2\sum_{i=1}^{N}\boldsymbol{w}_i\,|\,\boldsymbol{g}_i\,| + \|\,\boldsymbol{g} - \boldsymbol{v}^{k+1}\,\|^2/2\xi\right\}$.

3. End

4. The resultant solution is output.

Following the above deduction and analysis, the ISB method, the FBS technique and the ST method have been combined into a potent solver for Eq. (11), and Algorithm 2 provides the main computing steps.

Algorithm 2: Proposed solving procedure for equation (11)

1. The parameters for executing the algorithm are assigned.

2. For $k = 0,1,2,\cdots$, implement the following iterative loop

Step 1. Update $\boldsymbol{d}^{k+1}$ by equation (17).

Step 2. Update $\boldsymbol{v}^{k+1}$ by:

$$\boldsymbol{v}^{k+1} = \boldsymbol{g}^k - \xi(\boldsymbol{A}^T(\boldsymbol{A}\boldsymbol{g} - \boldsymbol{y}) + \beta\boldsymbol{D}^T(\boldsymbol{D}\boldsymbol{g} - \boldsymbol{D}\boldsymbol{g}_\ell + \boldsymbol{b}^k - \boldsymbol{d}^{k+1}))\,.$$

Step 3. Update $\boldsymbol{g}^{k+1}$ by:

$$\boldsymbol{g}^{k+1} = \min\left\{\lambda_2\sum_{i=1}^{N}\boldsymbol{w}_i\,|\,\boldsymbol{g}_i\,| + \|\,\boldsymbol{g} - \boldsymbol{v}^{k+1}\,\|^2/2\xi\right\}$$

Step 4. Update $\boldsymbol{b}^{k+1}$ by equation (14).

3. End

4. The resultant solution is output.

The proposed numerical method, Algorithm 2, has two distinct characteristics. On one hand, the ISB method is extended to search for a high quality solution of the devised optimization model with non-smooth regularizers. By taking advantage of the alternating optimization method and the variable splitting technique, the intractable optimization problem is separated into two sub-problems that can be easily solved, reducing the costly calculation. On the other hand, the ST algorithm and the FBS method are deployed as the sub-problem solvers for further lowering the costly computation, and thus the efficiency of computation is improved.

4. Ensemble least squares support vector machine

The most remarkable characteristic in the devised imaging model depends on the introduction of the LR. As a result, it is vital for our proposed imaging model to obtain a reliable prior image. We deploy a machine learning method to acquire a data-driven prior image in this study. The ensemble learning is one of excellent machine learning methods, has been widely and successfully applied to diverse scenarios and produces high quality results. Therefore, we design a new ensemble least squares support vector machine (ELSSVM) method to predict a prior image in this study. Concretely, the RP method is introduced to improve the diversity of ensemble, the LSSVM method serves as a base learner, and the SMR, which is solved by the DE method, is deployed to combine the ensemble of solution.

Table 1
Popular kernel functions.

Function name	Function form
Linear kernel	$\boldsymbol{K}(\boldsymbol{s},\boldsymbol{s}_i) = (\boldsymbol{s}^T\boldsymbol{s}_i)$
Polynomial kernel	$\boldsymbol{K}(\boldsymbol{s},\boldsymbol{s}_i) = (\boldsymbol{s}^T\boldsymbol{s}_i + 1)^d$
RBF kernel	$\boldsymbol{K}(\boldsymbol{s},\boldsymbol{s}_i) = \exp\left(-\frac{\|\boldsymbol{s}-\boldsymbol{s}_i\|^2}{2\sigma^2}\right)$
Sigmoid kernel	$\boldsymbol{K}(\boldsymbol{s},\boldsymbol{s}_i) = \tanh(\boldsymbol{s}^T\boldsymbol{s}_i + \tau)$

4.1. Least squares support vector machine

The LSSVM technique is a widely-used supervised machine learning method for regression or classification tasks [54,55], which has the advantageous properties, such as excellent generalizability performance, fast training, high accuracy, low computing complexity, and more. Following the above advantages, the prior image is predicted by the LSSVM method in this study.

Given a set of training sample pairs, $\{\boldsymbol{s}_i, \boldsymbol{z}_i\}_{i=1}^m$, and a function, $\phi(\cdot)$, the regression model in the LSSVM method can be formulated as [54,55]:

$$z(\boldsymbol{s}) = \boldsymbol{\omega}^T\phi(\boldsymbol{s}) + u \tag{21}$$

where $\boldsymbol{\omega}$ and u represent a weight vector and a constant, respectively.

The training of the LSSVM model can be cast into an optimization problem below:

$$\begin{cases}\min\left\{\frac{1}{2}\|\boldsymbol{\omega}\|^2 + \eta\frac{1}{2}\sum_{i=1}^{n}\boldsymbol{r}_i^2\right\} \\ s.t.\,\boldsymbol{z}_i = \boldsymbol{\omega}^T\phi(\boldsymbol{s}_i) + u + \boldsymbol{r}_i,\ i = 1,2,\ldots,n\end{cases} \tag{22}$$

where $\eta > 0$ stands for a penalty parameter.

The Lagrangian function of Eq. (22) can be written as follows:

$$L = \frac{1}{2}\|\boldsymbol{\omega}\|^2 + \eta\frac{1}{2}\sum_{i=1}^{n}\boldsymbol{r}_i^2 - \sum_{i=1}^{n}\boldsymbol{\rho}_i(\boldsymbol{\omega}^T\varphi(\boldsymbol{s}_i) + b + \boldsymbol{r}_i - \boldsymbol{z}_i) \tag{23}$$

where $\boldsymbol{\rho}_i$ are the Lagrange multipliers.

Finally, the solution of Eq. (22) means solving Eq. (23). Following the optimization principles, the solution of Eq. (23) is equivalent to solving the following linear equations:

$$\begin{bmatrix}0 & \boldsymbol{1}_n^T \\ \boldsymbol{1}_n & \boldsymbol{K} + \eta^{-1}\boldsymbol{I}\end{bmatrix}\cdot\begin{bmatrix}u \\ \boldsymbol{\rho}\end{bmatrix} = \begin{bmatrix}0 \\ \boldsymbol{y}\end{bmatrix} \tag{24}$$

where $\boldsymbol{K}(\boldsymbol{s}_i,\boldsymbol{s}_j) = \phi(\boldsymbol{s}_i)^T\phi(\boldsymbol{s}_j)$ is call as the kernel function.

The training of the LSSVM method means solving Eq. (24) using a proper method to obtain $\boldsymbol{\rho}_i$ and u. Once the estimations of the variables $\boldsymbol{\rho}_i$ and u are obtained, the resulting LSSVM model for the regression problem becomes:

$$z(\boldsymbol{s}) = \sum_{i=1}^{n}\boldsymbol{\rho}_i\boldsymbol{K}(\boldsymbol{s},\boldsymbol{s}_i) + u \tag{25}$$

Before deploying the LSSVM technique to actual problems, a proper kernel function needs to be determined in advance. Prevalent kernel functions involve linear, polynomial, RBF kernel, polynomial kernel, etc., and their function forms are given in Table 1.

Obviously, the training of the LSSVM model involves the preparation of training dataset, selection of kernel function and estimation of the model parameters. In Algorithm 3 we detail the calculation procedure for training the LSSVM model.

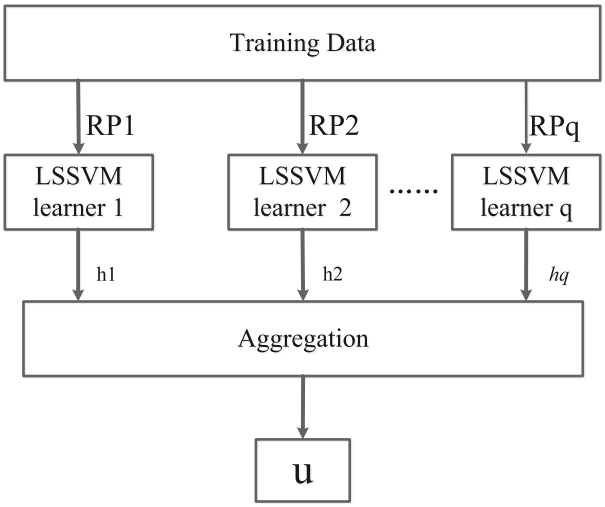

Fig. 1. Proposed ELSSVM method.

Algorithm 3: Training procedure of the LSSVM model

1. Determine the training samples.
2. Select the kernel function.
3. Construct the kernel matrix.
4. Estimate the variables ρ_i and u by solving equation (24).

It is worth mentioning that although the training of the LSSVM method is simple, it is still challenging when data volume is huge. In this case, relevant big data technologies, more effective training methods, such as parallel computing method, distributed computation method, graphics processing units based computing method, etc., should be used to solve the problem. We remain this as future study.

4.2. Random projection based dimensionality reduction

To obtain better perceptual quality, the image size is often large. For example, the size of an image is 32×32 in this study, which is rearranged into a vector with the dimensionality 1024×1. Directly feeding this vector into the LSSVM method will inevitably lead to increasing cost and load of computation. In order to reduce the redundancy of input images, decrease the difficulty in calculation and overcome the over-fitting, we employ the RP method to decrease the size of the original input data before they are used to train the LSSVM model.

In the RP method, the projection matrix is generated randomly, and thus the computation cost is significantly decreased [56–58]. In the RP method, the original data with the dimensionality d_1 is projected to a low dimensional subspace d_2 ($d_2 \ll d_1$) by a projection matrix $\boldsymbol{\psi}$ with the dimensionality $d_2 \times d_1$ [56], and the process is formulated as:

$$\boldsymbol{S}^{RP}_{d_2 \times M} = \boldsymbol{\psi}_{d_2 \times d_1} \boldsymbol{S}_{d_1 \times M} \tag{26}$$

where $\boldsymbol{S}_{d_1 \times M} = [\boldsymbol{s}_1, \boldsymbol{s}_2, \ldots, \boldsymbol{s}_M]$ stands for the original dataset with the dimensionality d_1; $\boldsymbol{S}^{RP}_{d_2 \times M}$ means the low dimensional projection data.

Reducing dimensionality with the RP technique has two main steps. First, the projection matrix is generated randomly. Second, the generated projection matrix is used to reduce the size of the input data by implementing a matrix multiplication operation. Algorithm 4 summarizes the computing steps for the RP-based dimensionality reduction method [56].

To reduce the costly computation and improve the performance, instead of feeding the original samples to the LSSVM model, in this study the size reduction data, i.e., $\boldsymbol{S}^{RP}_{d_2 \times M}$, is used to train the LSSVM model.

4.3. Ensemble LSSVM

Following the imaging model (Eq. (11)), it is crucial to seek for an effective method to predict a prior image. The ensemble learning method is regarded to be a state-of-the art solution for a wide range of applications across different tasks and areas [59,60]. The ensemble learning method assumes that the final forecasting quality can be improved by combining the results from multiple base learners.

In this study we develop an effective ensemble learning method that leverages the advantageous properties of the RP method, the LSSVM method and the SMR. The main idea of the proposed ensemble learning method, named the ensemble least squares support vector machine (ELSSVM), is to increase the forecasting accuracy via ameliorating the diversity of ensemble. Specifically, the RP is deployed to capture the ensemble of data features via setting different dimensionalities of feature, the LSSVM method is tailored to fulfill the supervised learning to produce a forecasting ensemble that will be combined into a final prior image by the SMR method that lays stress on the sparseness of the regression coefficients. In the ELSSVM method, the diversity of ensemble is ameliorated by introducing the feature ensembles with the RP method. For intuitive understanding, we show the ELSSVM structure in Fig. 1.

Following the above discussion, Algorithm 5 outlines the computing steps in training the ELSSVM method. Finally, the LSSVM parameters and the coefficients in the SMR method will be obtained via implementing the algorithm.

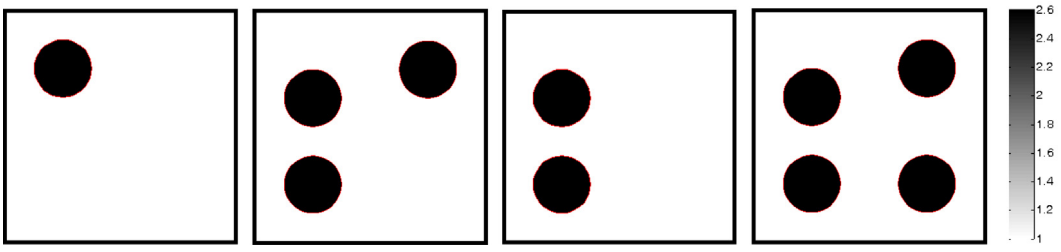

Fig. 2. Reconstruction targets.

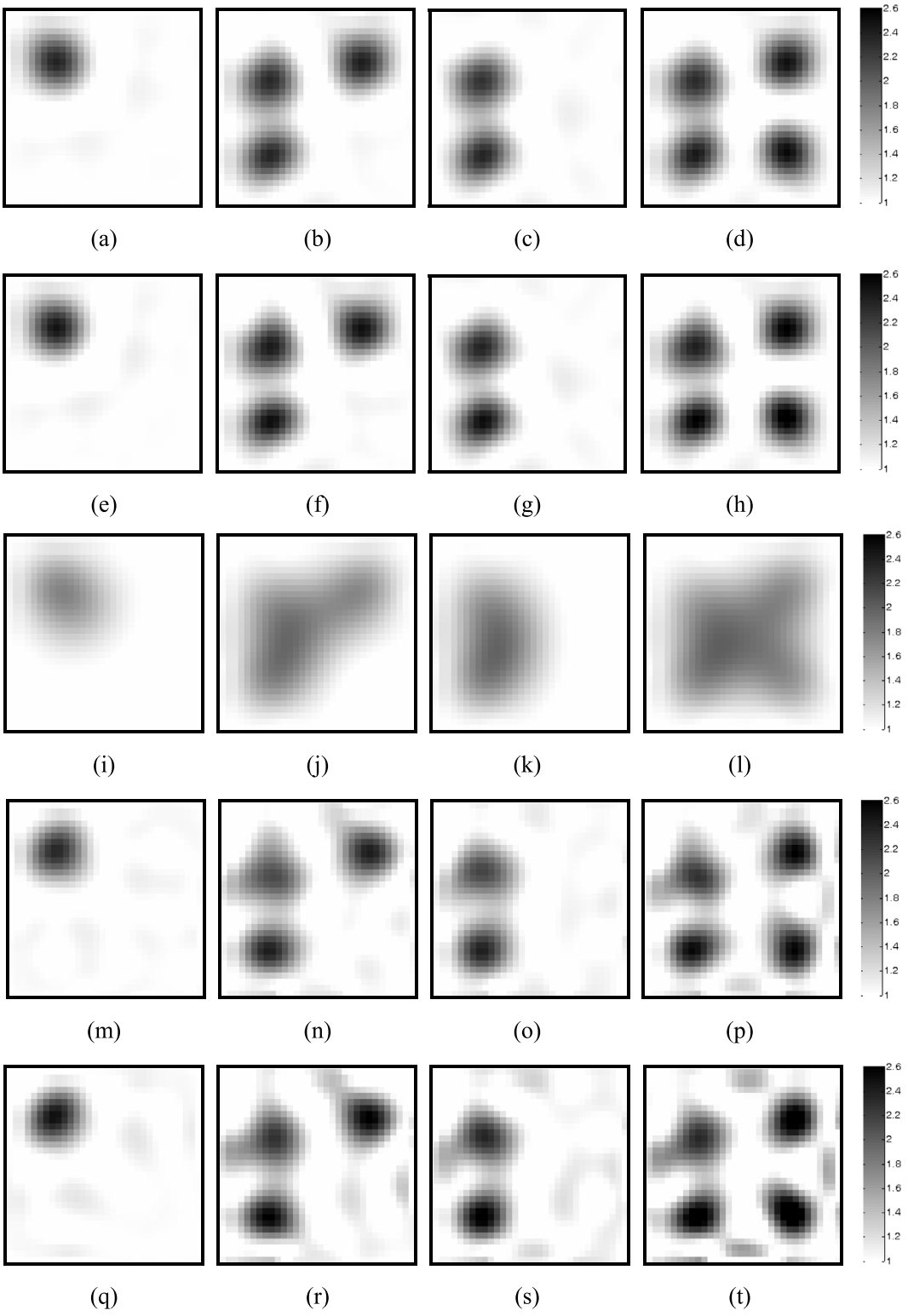

Fig. 3. Performance testing of the non-iterative methods. (a–d, e–h, i–l, m–p and q–t demonstrate the results recovered by the L2R algorithm, the OIOR algorithm, the LBP algorithm, the FR algorithm and the TSVD algorithm, respectively.)

4.4. Sparse matrix regression

To aggregate the solutions from the base learners, in this study we develop the SMR method that imposes the sparseness of the regression coefficients, which is solved by the DE method.

Given a true image $\boldsymbol{R}$ and q images, $\boldsymbol{h}_1, \boldsymbol{h}_2, \ldots, \boldsymbol{h}_q$, which come from the LSSVM base learners. We assume that the true image $\boldsymbol{R}$ can be linearly represented by $\boldsymbol{h}_1, \boldsymbol{h}_2, \ldots, \boldsymbol{h}_q$, i.e.,

$$\boldsymbol{R} = \theta_1 \boldsymbol{h}_1 + \theta_2 \boldsymbol{h}_2 + \cdots + \theta_q \boldsymbol{h}_q + \boldsymbol{\varepsilon} \tag{27}$$

where $\theta_1, \theta_2, \ldots, \theta_q$ are defined as the representation coefficients and $\boldsymbol{\varepsilon}$ means the fitting error.

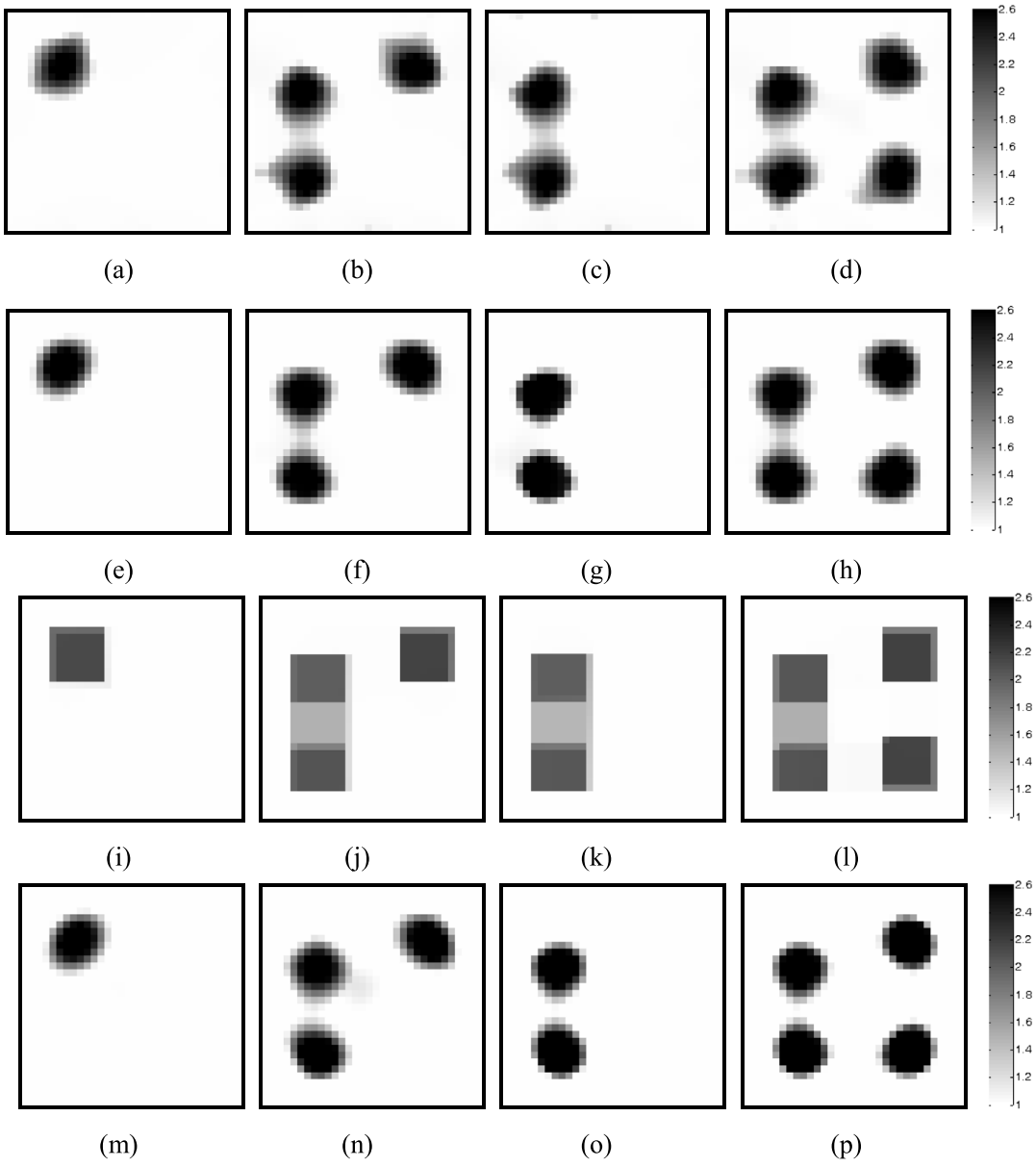

Fig. 4. Performance testing of the iterative methods. (a–d, e–h, i–l, m–p, q–t, u–x, y–ab and ac-af demonstrate the results recovered by the ART, the CIP algorithm, the TVR algorithm, the L1R algorithm, the IL algorithm, the FRCG algorithm, the SKI algorithm and the LRR algorithm, respectively.)

By introducing a new notation, $\boldsymbol{H\theta} = \theta_1\boldsymbol{h}_1 + \theta_2\boldsymbol{h}_2 + \cdots + \theta_q\boldsymbol{h}_q$, where $\boldsymbol{\theta} = [\theta_1, \theta_2, \ldots, \theta_q]^T$, Eq. (27) becomes:

$$\boldsymbol{R} = \boldsymbol{H\theta} + \boldsymbol{\varepsilon} \tag{28}$$

To increase the quality of a solution, Eq. (28) is transformed into an optimization problem below:

$$\min_{\boldsymbol{\theta}} f(\boldsymbol{\theta}) \tag{29}$$

where $f(\boldsymbol{\theta}) = \sum_{\ell=1}^{M} \|\boldsymbol{H}_\ell\boldsymbol{\theta} - \boldsymbol{R}_\ell\|_1 + \lambda\|\boldsymbol{\theta}\|_1$; $\sum_{\ell=1}^{M} \|\boldsymbol{H}_\ell\boldsymbol{\theta} - \boldsymbol{R}_\ell\|_1$ measures the data fidelity and $\|\boldsymbol{\theta}\|_1$ enforces the sparseness of the regression coefficients.

It is interesting for the proposed ELSSVM method to find a powerful method to solve Eq. (29). The DE algorithm is a population-based stochastic optimization method that does not require the differentiability of a cost function [61,62]. Currently, the DE method has found applications across different tasks and domains, and high quality solutions have been found owing to its advantageous numerical behaviors, such as good global search performance, excellent robustness, and more. As a consequence, the DE algorithm is tailored to solve Eq. (29) in this work, and the main computing steps are summarized in Algorithm 6. More theoretical background and technical details can refer to [61–67].

5. Proposed reconstruction scheme

In previous sections, we have devised a potent optimization model for imaging, and developed a simple but powerful hybrid solver. The developed method involves two key stages: the prediction of a prior image and the solution of the inverse problem. Particularly, the forecast of a prior image is decoupled from the solution of the inverse problem.

The developed algorithm is detailed in Algorithm 7, and it is called the learned regularization reconstruction (LRR) technique.

We qualitatively characterize the developed LRR method below:

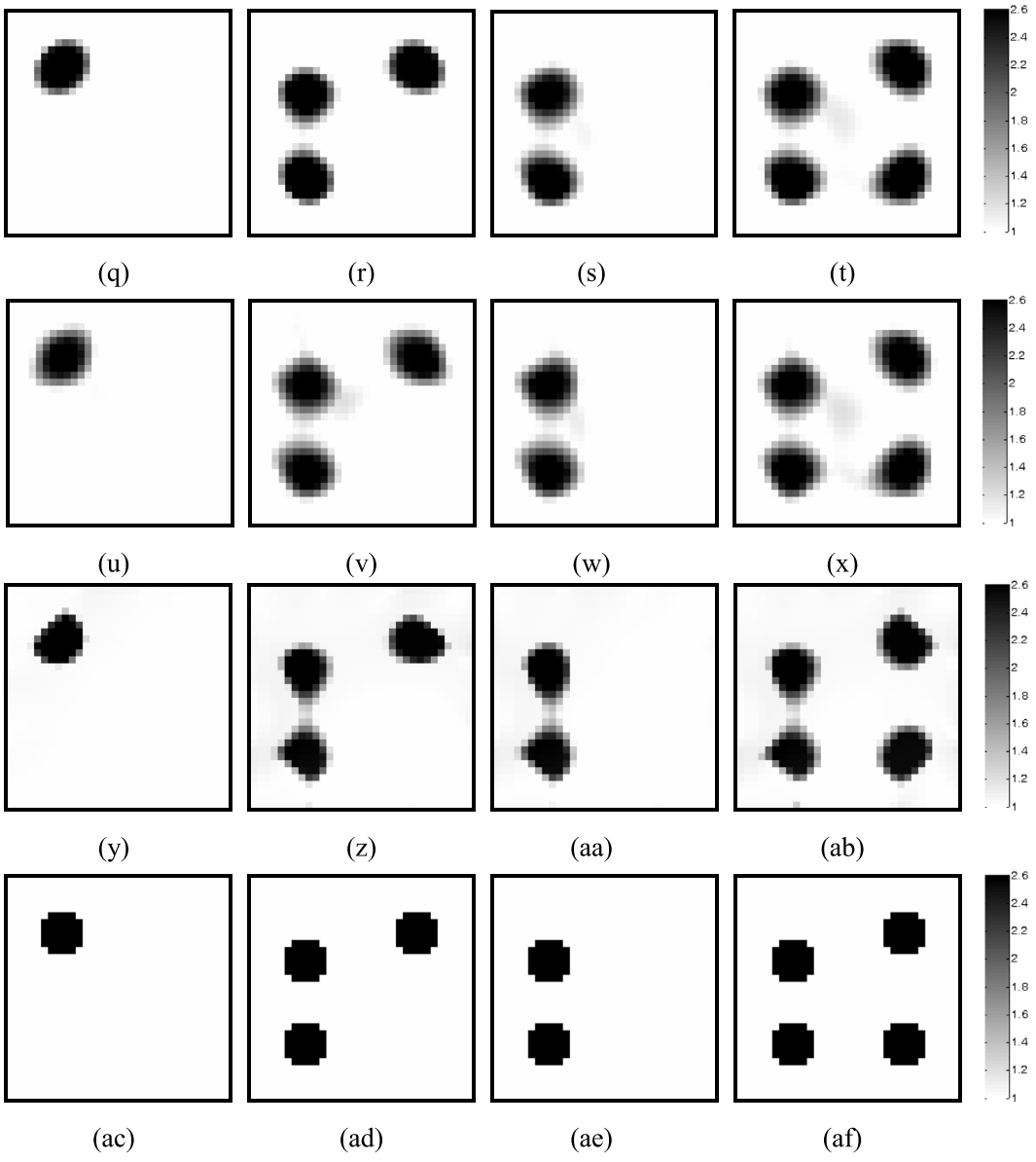

Fig. 4. (*continued*).

Algorithm 4: RP-based dimensionality reduction method

1. Generate a stochastic matrix, in which each entry satisfies the normal distribution, and its mean and variance are set to 0 and 1, respectively.
2. Carry out the orthogonalization to the each row of the generated stochastic matrix by the Gram-Schmidt algorithm, and then normalize them to unit length, finally yield a resulting RP matrix.
3. Reduce the dimensionality of the original data by implementing equation (26).

(1) The sparsity prior and the LR from the ELSSVM method are introduced to increase the elasticity in the exploitation of the prior knowledge, which are combined into a new computing imaging model. Reconstruction artifacts can be reduced by integrating the potent image priors into an imaging model.

(2) A simple but powerful solver is developed by integrating the FBS algorithm and the ST method into the ISB algorithm, which is used to efficiently solve the cost function devised in this study. The introduction of the FBS method and the ST method will significantly reduce the costly calculation.

(3) A potent ensemble learning method, named the ELSSVM method, is developed to forecast a high reliability prior image, which provides a solid foundation for reducing reconstruction errors. In the proposed ELSSVM method, the RP is deployed to

Algorithm 5: Proposed ELSSVM

1. The parameters for executing the algorithm are assigned and the training dataset is given.

2. Generate the feature ensemble.

The RP method is deployed to the input data, and thus the training samples are composed of $(\boldsymbol{l}_i^j, \boldsymbol{z}_i)_{i=1}^M$, where $\boldsymbol{l}_i^j = \boldsymbol{\psi}^j \boldsymbol{s}_i$, $i = 1, 2, \cdots, M$ stands for the index of training dataset, $j = 1, 2, \cdots, K$ represents different ensembles of features and $\boldsymbol{\psi}^j$ stands for the jth RP matrix.

3. Train LSSVM model.

Train the jth LSSVM model by the feature ensemble and corresponding sample labels, i.e., $(\boldsymbol{l}_i^j, \boldsymbol{z}_i)_{i=1}^M$.

4. Aggregate the solutions from the base learners.

The solutions from the LSSVM learners are aggregated by the SMR method.

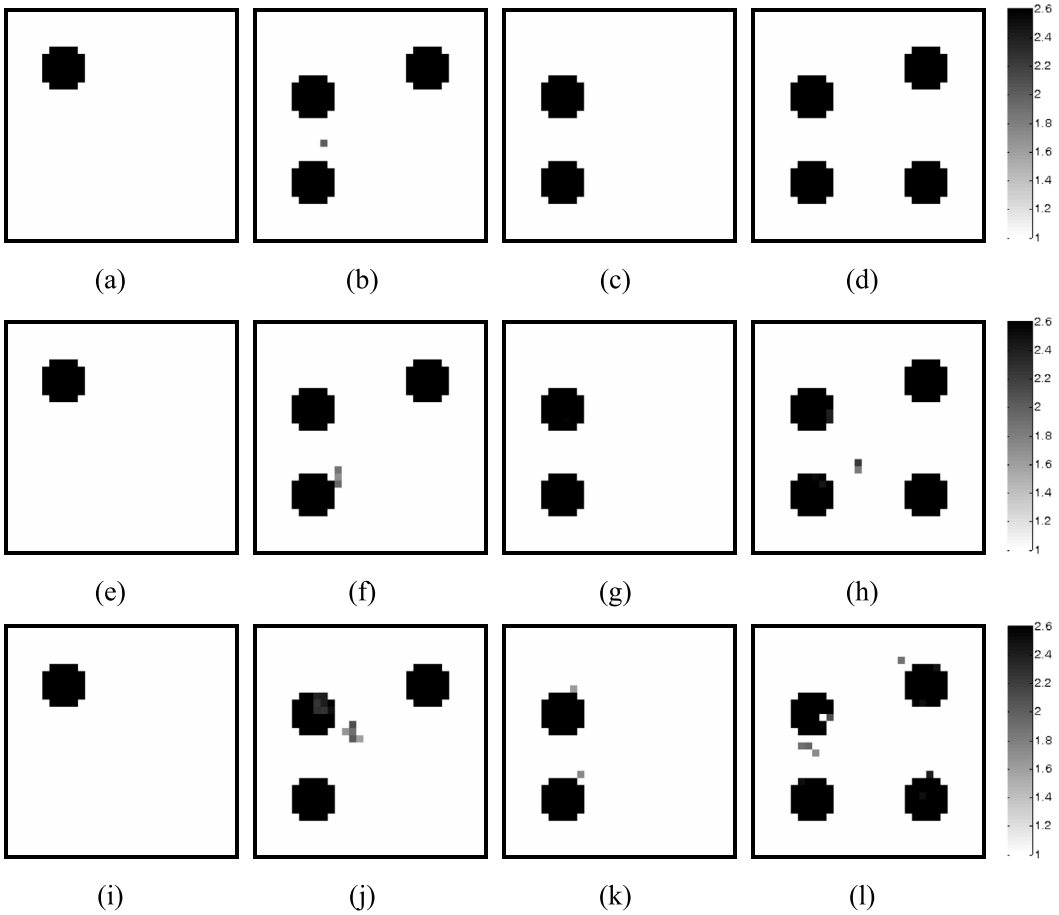

Fig. 5. Performance testing of the LRR algorithm with noisy capacitance data. (a–d, e–h and i–l demonstrate the results recovered by the LRR algorithm under different LoNs, i.e., 5%, 10% and 15%, respectively.)

capture an ensemble of data feature, the LSSVM method is used as an effective base learner to obtain a forecasting ensemble, which are aggregated into a final prior image by the SMR method with the focus on the sparseness of the regression coefficients.

6. Experiment and discussion

To fulfill comprehensive and fair performance testing, the LRR algorithm is numerically tested by carrying out the RQ comparison with the widely-used algorithms listed in Table 2. Meanwhile,

Algorithm 6: Differential evolution algorithm

1. The number of individuals, *Num*, the number of generations, *MaxGen*, and other parameters for executing the algorithm, such as I_{CR} and I_F, are specified.

2. Let $NoI = 0$.

3. The initial population $\boldsymbol{\theta}_{i,NoI}$, $i = 1, 2, \cdots, Num$, is generated.

4. The cost function $f(\boldsymbol{\theta}_{i,NoI})$ (equation (29)) is evaluated.

5. For $NoI = 1$ to *MaxGen*

For *i*=1 to *Num* implement

Randomly choose $c1 \neq c2 \neq c3$.

RanInt=randint(1,*p*)

For *j*=1 to *p* do

If (*RanNum*(0,1)< I_{CR} or *j*= *RanInt*) then

$$\boldsymbol{o}_{i,j,NoI+1} = \boldsymbol{\theta}_{c3,j,NoI} + I_F(\boldsymbol{\theta}_{c1,j,NoI} - \boldsymbol{\theta}_{c2,j,NoI})$$

Else

$$\boldsymbol{o}_{i,j,NoI+1} = \boldsymbol{\theta}_{i,j,NoI}$$

End if

End for

If $f(\boldsymbol{o}_{i,NoI+1}) < f(\boldsymbol{\theta}_{i,NoI})$ Then

$$\boldsymbol{\theta}_{i,NoI+1} = \boldsymbol{o}_{i,NoI+1}$$

Else

$$\boldsymbol{\theta}_{i,NoI+1} = \boldsymbol{\theta}_{i,NoI}$$

End if

End for

$NoI \leftarrow NoI + 1$

End for

the sensitivities of the LRR method to the noisy capacitance data and the selection of the regularization parameter value are also tested.

In order to fulfill the numerical validation, we simulate a widely-used 12-electrode square sensor, and details on the geometric configuration and size can refer to [28].

In our simulations, the LSSVM employs the polynomial kernel function, and the model parameters are determined by the 10-fold cross-validation method. The sizes of the RP matrices are 64 ×1024, 128×1024, 300×1024, 512× 1024 and 700 × 1024, respectively. In the DE algorithm, the number of population is 30, $I_F = 0.5$ and $I_{CR} = 0.5$. This work takes advantage of the MATLAB to fulfill the training of the ELSSVM model as well as all the tested solvers.

This study uses the noisy capacitance vector to assess the tested methods, and the definition of the level of noise (LoN) can refer to [28]. Additionally, the widely-used performance measurement criterion, the image error (IE) defined in [28], is used to assess the solvers listed in Table 2.

6.1. Case 1

This section carries out experiments on the RTs (Fig. 2) that are frequently used in the ECT community. The step size (SS) of the ART is 1, and the numbers of iterations (NoIs) with regard to the RTs in Fig. 2(a)–(d) are 269, 318, 322 and 400, respectively. The SS of the CIP technique is 1, and the NoIs with regard to the RTs in Fig. 2(a)–(d) are 386, 408, 475 and 908, respectively. The SS of the IL technique is also 1, and the NoIs with regard to the RTs in Fig. 2(a)–(d) are 324, 448, 504 and 432, respectively. In the above settings for the ART, the CIP algorithm and the IL technique, the minimum IEs are obtained for ensuring the fair and objective comparison. The exponential value in the FR method is set to 0.1. The threshold value of the truncated singular

Algorithm 7: Proposed LRR method

1. The parameters for executing the algorithm are assigned.
2. Training datasets, including input and output data, are provided. The input data refers to the images recovered by the IL algorithm, and the output data is the true target images.
3. Algorithm 4 is carried out to decrease the size of the training data.
4. Train the ELSSVM model via Algorithm 5.
5. Feed a testing capacitance vector to the IL method, yielding a preliminary image.
6. Reduce the size of the preliminary image by Algorithm 4, which is further used to forecast a prior image by the trained ELSSVM model.
7. According to the learned prior image, deploying Algorithm 1 to solve equation (11) for generating a resulting reconstruction.

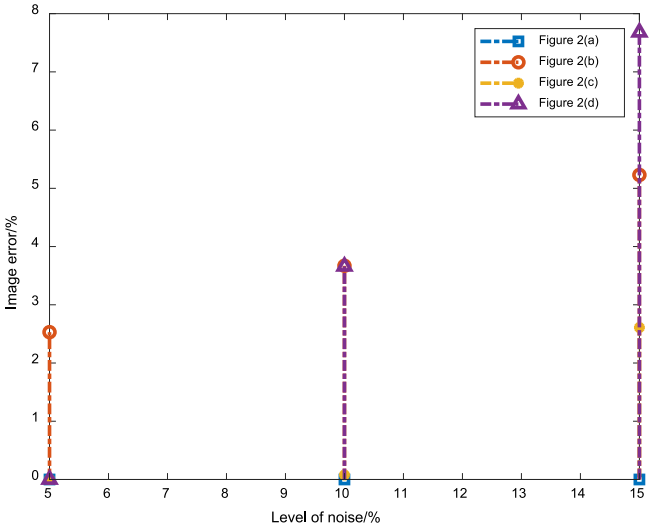

Fig. 6. Image errors of the LRR method using the capacitance data with different LoNs.

Table 2
Compared imaging methods.

Algorithms	Attribute
LBP/Linear back projection	Non-iterative algorithm
L2R/L_2 norm regularization	Non-iterative algorithm
OIOR/Offline iteration online reconstruction	Non-iterative algorithm
FR/Fractional regularization	Non-iterative algorithm
TSVD/Truncated singular value decomposition	Non-iterative algorithm
ART/Algebraic reconstruction technique	Iterative algorithm
FRCG/Fletcher–Reeves conjugate gradient	Iterative algorithm
TVR/Total variation regularization	The cost function is iteratively solved by the ISB algorithm
CIP/Cimmino iterative projection	Iterative algorithm
L1R/L_1 norm regularization	The cost function is iteratively solved by the fast iterative shrinkage-thresholding algorithm
SKI/Sparse Kaczmarz iteration	Iterative algorithm
IL/ Iteration Landweber	Iterative algorithm

value in the TSVD method is 0.003. To obtain a good result, the regularization parameter values with regard to the L2R algorithm, the L1R technique and the TVR method are set to 0.003, 0.01 and 0.008, respectively. In the LRR solver, $\boldsymbol{W}_{ii}^{k+1} = 1/(|\boldsymbol{g}_i^k|^4 + 10^{-10})$ is a diagonal matrix, $\lambda_1 = 0.001$, $\lambda_2 = 0.004$, and the termination criterion is set to $\|\boldsymbol{g}^{k+1} - \boldsymbol{g}^k\|/\|\boldsymbol{g}^k\| \leq 10^{-4}$. The L2R technique is carried out to provide the starting solutions for the iterative solvers. The resulting results recovered by the non-iterative and iterative solvers are summarized in Figs. 3 and 4, respectively. Table 3 provides the IEs for comparison.

Following the comparisons summarized in Figs. 3 and 4, it is verified that the LRR method produces the better reconstructions than the other tested solvers. Three main reasons result in these impressive results. First, a flexible optimization model is devised, and it leverages the prior image forecasted by the proposed

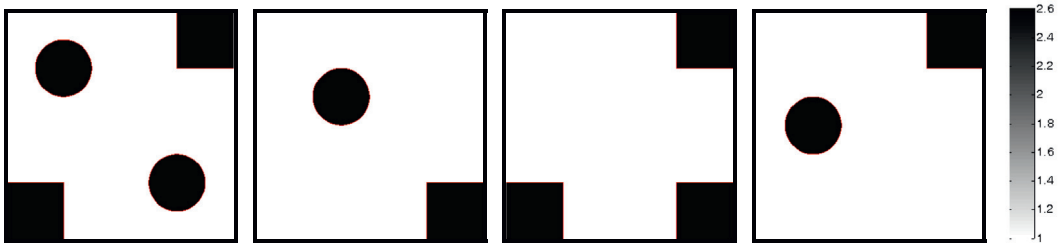

Fig. 7. Reconstruction targets.

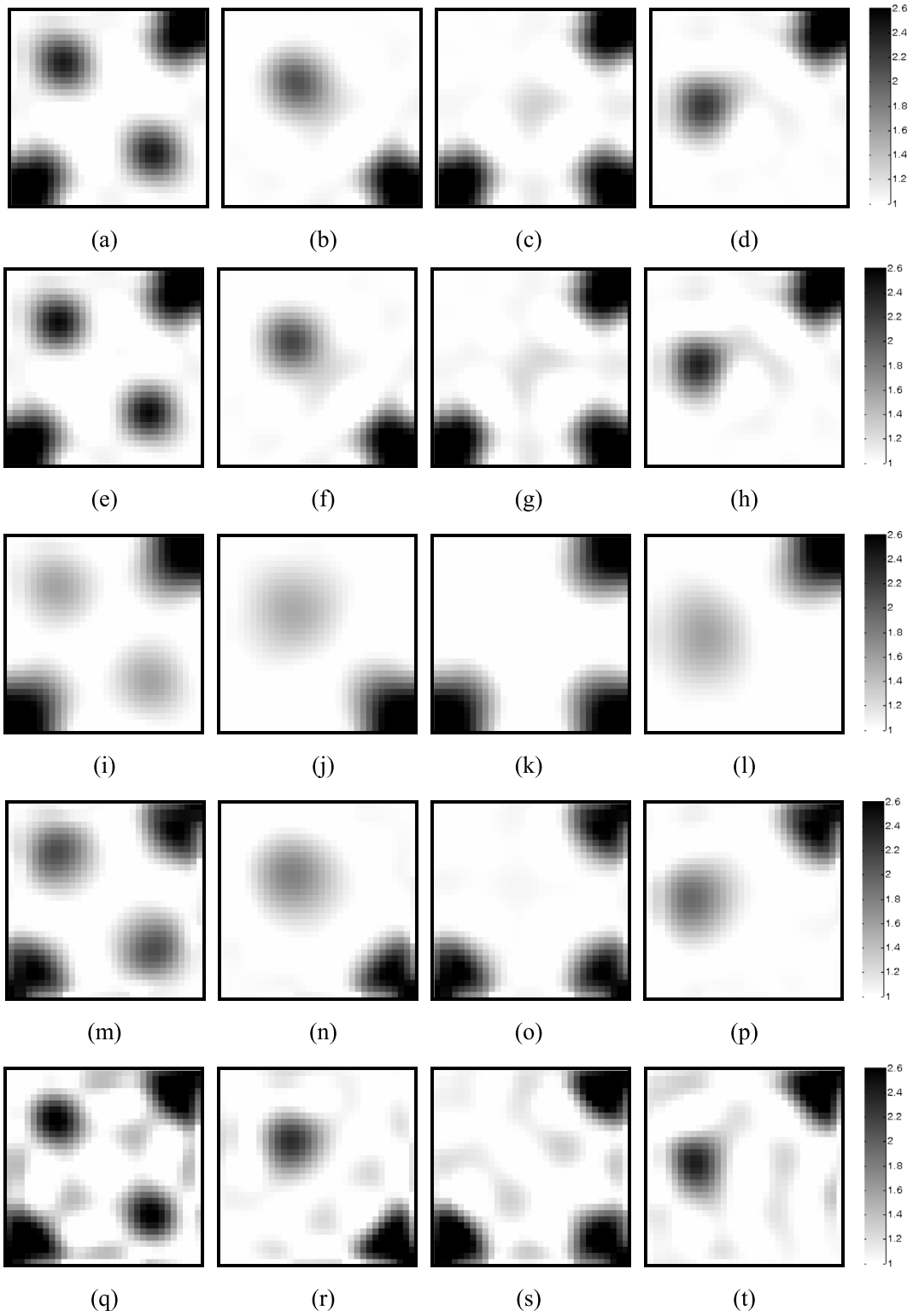

Fig. 8. Performance testing of the non-iterative methods. (a–d, e–h, i–l, m–p and q–t demonstrate the results recovered by the L2R algorithm, the OIOR algorithm, the LBP algorithm, the FR algorithm and the TSVD algorithm, respectively.)

ELSSVM method and the prior about sparseness. Numerical experiments have validated that the imaging model devised in this study provides a powerful way for capitalizing on image priors. Second, the FBS method and the ST technique are inserted into the ISB method to yield a potent hybrid solver for the developed optimization model. Actual reconstructions have verified that the proposed hybrid solver can reduce the costly computation and stabilize the solution process. Third, the ELSSVM method is deployed to forecast a prior image. Numerical experiment results have confirmed that the ELSSVM method is competent in forecasting a reliable prior image, which provides a solid foundation for reducing reconstruction artifacts. In actual reconstructions, it has been verified that the learned prior image does reduce reconstruction artifacts by the regularization technique.

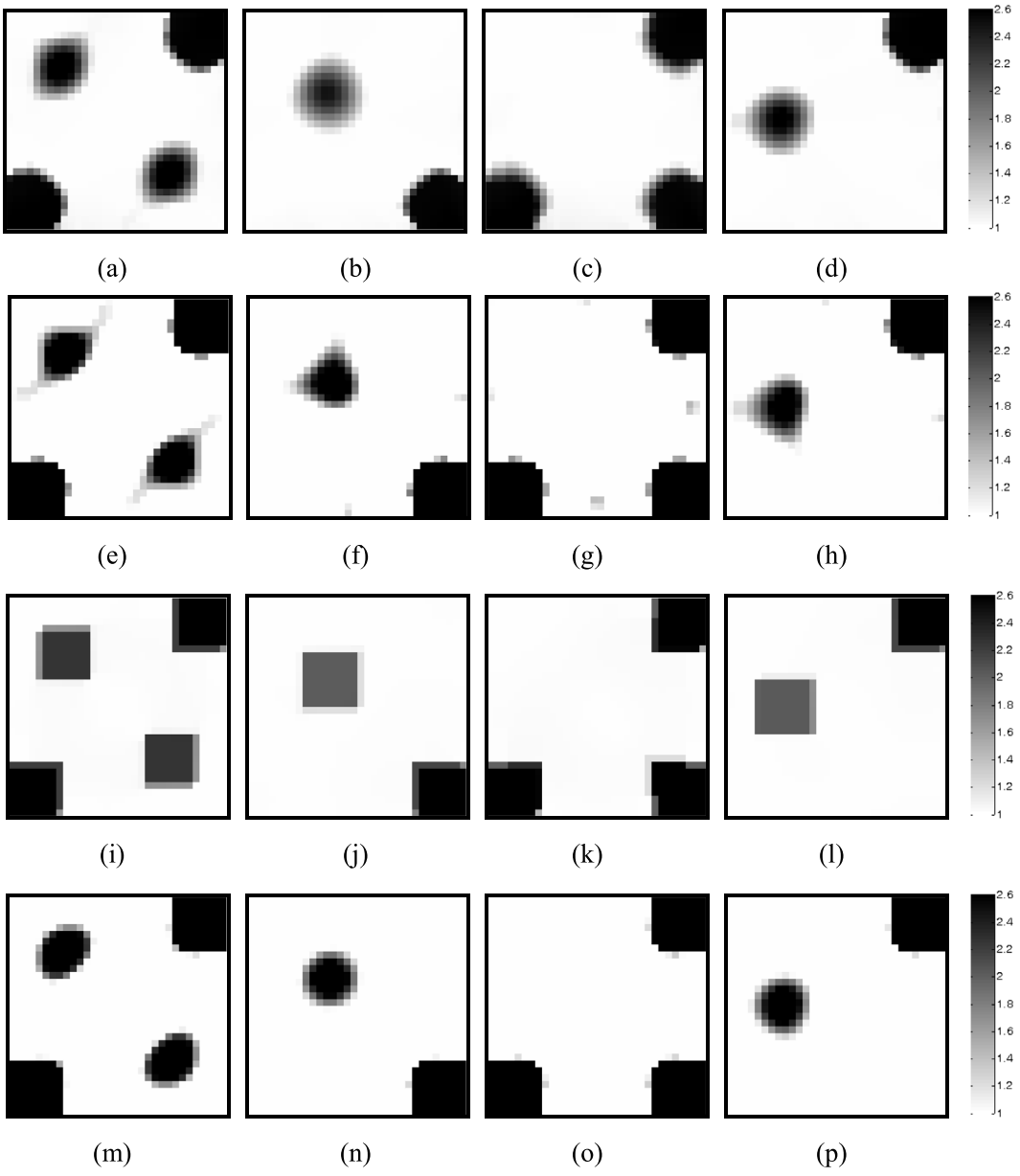

Fig. 9. Performance testing of the iterative methods. (a–d, e–h, i–l, m–p, q–t, u–x, y–ab and ac–af demonstrate the results recovered by the ART, the CIP algorithm, the TVR algorithm, the L1R algorithm, the IL algorithm, the FRCG algorithm, the SKI algorithm and the LRR algorithm, respectively.)

Table 3
Image errors with regard to the RTs in Fig. 2 (%).

Algorithms	Fig. 2(a)	Fig. 2(b)	Fig. 2(c)	Fig. 2(d)
L2R	16.13	24.23	21.06	25.85
OIOR	15.76	23.63	20.30	25.32
LBP	21.73	36.53	31.37	41.76
FR	14.44	24.31	21.29	24.70
TSVD	15.03	24.40	20.94	25.94
ART	12.26	18.57	16.37	20.13
CIP	11.44	17.30	15.18	18.98
TVR	18.62	27.74	24.42	29.91
L1R	10.60	15.75	13.48	21.69
IL	11.59	17.50	15.09	18.82
FRCG	11.65	17.68	15.36	19.05
SKI	11.08	15.56	12.87	16.86
LRR	≈0	≈0	≈0	≈0

As summarized in Table 3, the LRR algorithm fulfills the smaller IEs than the other tested solvers, and the recovered images are in a close proximity to the RTs. With regard to the non-iterative solvers, the IEs of the LBP method is the largest, but the IEs of the other non-iterative solvers are similar. Additionally, we can see that the reconstruction methods with the sparseness constraint, like the L1R technique and the SKI method, outperform the non-iterative algorithms, but are still inferior to the LRR method. These impressive reconstruction precisions have confirmed that the LRR method outperforms over the other tested solvers and is adept at reducing reconstruction artifacts and weakening deformations.

6.2. Case 2

The imprecise measurement in the capacitance data very likely occur in the process of the acquisition and transmission of signal, and it will be appropriate to use the imprecise capacitance data to test the LRR technique. In this section, the noise-perturbed capacitance data with different LoNs (5%, 10%, and 15%) are fed to the

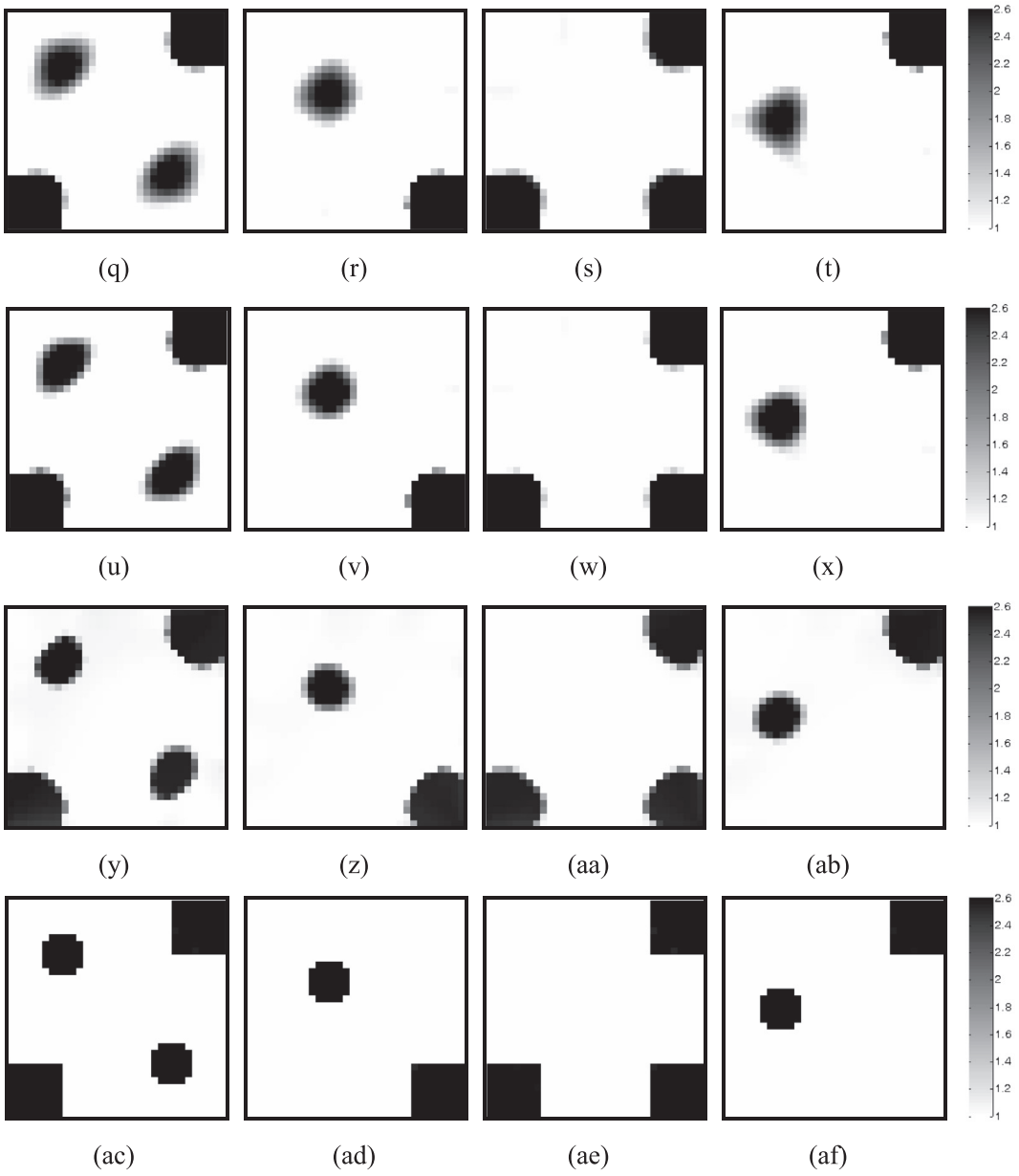

Fig. 9. (*continued*).

LRR algorithm to test its numerical behaviors. Fig. 5 summarizes the recovered results, and the IEs are given in Fig. 6.

According to Fig. 5, it has been verified that the LRR algorithm behaves well when the LoNs of the capacitance data are 5%, 10% and 15%. These good results can be explained from two aspects. First, the regularized cost function is devised to stabilize the computing process. Evidences from theoretical analysis and actual reconstructions have confirmed that the regularization technique is adept at stabilizing a solution. Second, taking advantage of the LR and the prior about sparseness contributes to reducing reconstruction artifacts. Many studies, including our experiments, have verified the significance of the prior information in reducing reconstruction artifacts and weakening deformations. In Fig. 6, we have found that the recovered images under different LoNs are still highly similar to the RTs, and the details about the edges and shapes of the permittivity distribution are still clear and distinguishable. As an instance, with the LoN of 15%, the IEs, 0, 5.23%, 2.61% and 7.68% with regard to the RTs in Fig. 2(a)–(d), respectively, are still relatively small. The testing results summarized in Table 4 have verified that the LRR method could alleviate the adverse impact that the capacitance noises bring on resulting reconstructions.

This study merely makes use of the noisy capacitance data to test the LRR algorithm. It is noteworthy that many factors influence the quality of recovered images in actual applications, and future studies should further test the proposed imaging technique using more experiment or simulation cases.

6.3. Case 3

We carry out another more intractable test on the challenging RTs summarized in Fig. 7. The SS in the ART is 1, and the NoIs with regard to the RTs in Fig. 7(a)–(d) are 72, 74, 21 and 77, respectively. The SS in the CIP technique is set to 1, and the NoIs with regard to the RTs in Fig. 7(a)–(d) are 471, 716, 520 and 463, respectively. The SS in the IL technique is also set to 1, and the NoIs with regard to the RTs in Fig. 7(a)–(d) are 130, 710, 79 and 533, respectively. The exponential value in the FR method is set to 0.5. The settings of the other tested solvers in this case and Case

Table 4
Image error comparison with regard to the RTs in Fig. 7 (%).

Algorithms	Fig. 7(a)	Fig. 7(b)	Fig. 7(c)	Fig. 7(d)
L2R	21.65	18.57	15.51	17.95
OIOR	21.08	18.12	15.32	17.58
LBP	25.07	21.71	16.73	21.92
FR	24.07	21.57	18.97	20.81
TSVD	22.12	19.76	18.16	20.18
ART	16.60	15.38	12.39	14.46
CIP	13.48	11.33	7.75	11.96
TVR	19.65	17.55	6.28	18.17
L1R	13.27	9.97	6.16	10.22
IL	14.29	11.59	7.20	11.81
FRCG	14.58	10.80	6.28	11.82
SKI	15.84	11.93	14.60	10.63
LRR	0.16	0.21	0.30	0.14

1 are the same. The recovered images are presented in Figs. 8 and 9, and the IEs are given in Table 4.

Following the recovered images summarized in Figs. 8 and 9, we have observed that the LRR method outperforms over the other tested solvers and produces better reconstructions, because a potent optimization model, i.e., Eq. (11), is put forward, a high-quality prior image is forecasted by the developed ELSSVM method and a new hybrid solver is developed to solve the devised optimization model efficiently. As expected, in the light of the comparison results provided by Table 4, it has been verified that the LRR method yields the highest reconstruction accuracy among all the tested solvers.

This work puts forward a potent imaging algorithm, and impressive recovery results have been obtained. It is noteworthy that the developed method can also be used for other imaging problems, such as electrical resistance tomography, acoustic tomography, electrical impedance tomography, electromagnetic tomography, etc. With the arrival of the era of big data, future research should further test the developed algorithm using more challenging cases and larger datasets.

6.4. Case 4

In addition to testing the recovery performance, this section also appraises the behaviors of the LRR method to different regularization parameter values, and the testing results are summarized in Fig. 10.

The selection of the regularization parameter value has a significant impact on the quality of a solution. Following the comparison results summarized in Fig. 10, it has been verified that different IE values appear with the variation of the regularization parameter values, but the variation tendency still remains a relatively stable level when the variation range of the regularization parameter value is large. The results have confirmed and clarified that the performances of the proposed LRR algorithm are not susceptible to the fluctuation of the regularization parameter value. This attribute is particularly beneficial to actual applications.

7. Conclusions

A potent LRR algorithm is developed to fulfill the goal of reducing reconstruction artifacts in this work. The improvement of performance relies mainly on three advantageous properties. First, a flexible model taking advantage of the LR predicted by the ELSSVM method and the prior about sparseness is developed for imaging. The model provides a potent approach for capitalizing on image priors. Second, the ISB method is extended into a potent hybrid solver for the developed imaging model by leveraging the FBS method and the ST method to solve subproblems efficiently. Third, the ELSSVM method is developed to

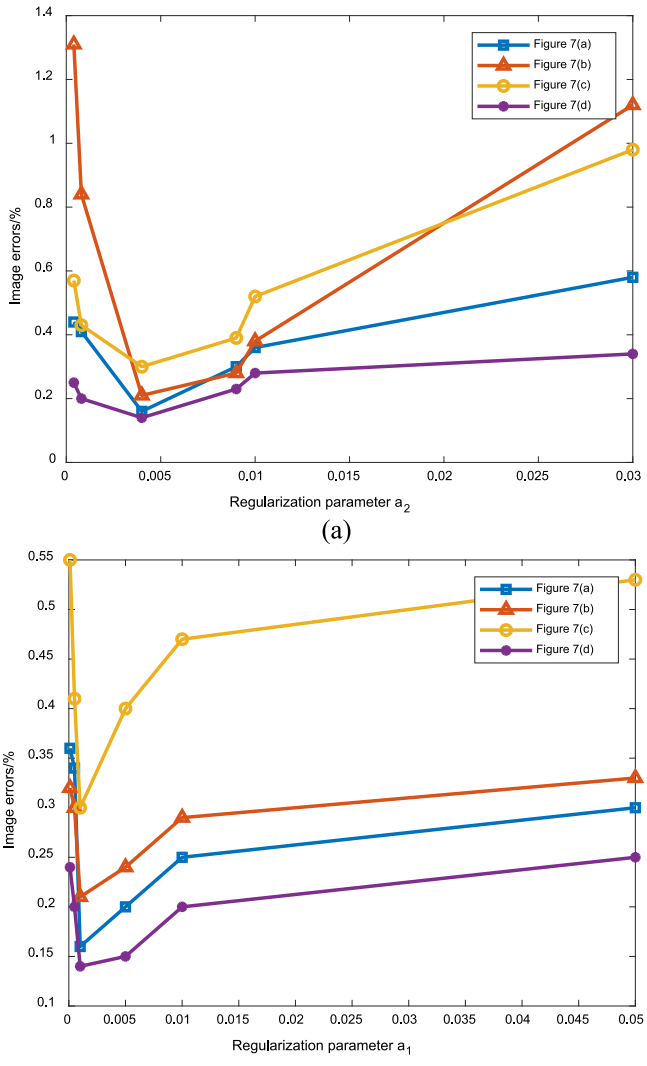

Fig. 10. Image errors of the LRR algorithm with regard to different regularization parameter values. (a. The variation trend of the IEs with regard to the RTs in Fig. 7(a)–(d) with the fixed $\alpha_1 = 0.001$; b. The variation trend of the IEs with regard to the RTs in Fig. 7(a)–(d) with the fixed $\alpha_2 = 0.004$.)

forecast a reliable learned prior image, which provides a solid foundation for the improvement in the quality of a solution. Especially, these research achievements in this work have clarified that reconstruction artifacts and deformations can be reduced by simultaneously leveraging the domain knowledge and the priors from example learning.

Declaration of competing interest

No author associated with this paper has disclosed any potential or pertinent conflicts which may be perceived to have impending conflict with this work. For full disclosure statements refer to https://doi.org/10.1016/j.asoc.2020.106126.

Acknowledgments

This authors would like to acknowledge the financial support from the National Natural Science Foundation of China (Nos. 51206048 and 51576196), the Fundamental Research Funds for

the Central Universities (No. 2017MS012) and the National Key Research and Development Program of China (No. 2017YFB0903601).

References

[1] A.N. Tikhonov, V.Y. Arsenin, Solution of Ill-Posed Problems, V.H. Winston & Sons, New York, 1977.
[2] S. Liu, L. Fu, W.Q. Yang, H.G. Wang, F. Jiang, Prior-online iteration for image reconstruction with electrical capacitance tomography, IEE Proc.-Sci. Meas. Technol. 151 (2004) 195–200.
[3] P.C. Hansen, Truncated singular value decomposition solutions to discrete ill-posed problems with ill-determined numerical rank, SIAM J. Sci. Stat. Comput. 11 (1990) 503–518.
[4] Z. Cao, L.J. Xu, H.X. Wang, Electrical capacitance tomography with a non-circular sensor using the dbar method, Meas. Sci. Technol. 21 (2010) 1–6.
[5] H. Yan, Y.F. Wang, Y.G. Zhou, Y.H. Sun, 3D ECT Reconstruction by an improved landweber iteration algorithm, Flow Meas. Instrum. 37 (2014) 92–98.
[6] R. Martin, V. Ogarko, D. Komatitsch, M. Jessell, Parallel three-dimensional electrical capacitance data imaging using a nonlinear inversion algorithm and L^pnorm-based model regularization, Measurement 128 (2018) 428–445.
[7] C.T. Shih, Y.J. Chang, J.T. Hsu, K.S. Chuang, S.J. Chang, J. Wu, Image reconstruction of optical computed tomography by using the algebraic reconstruction technique for dose readouts of polymer gel dosimeters, Phys. Medica 31 (2015) 942–947.
[8] X.Y. Dong, Z.Y. Ye, M. Soleimani, Image reconstruction for electrical capacitance tomography by using soft-thresholding iterative method with adaptive regulation parameter, Meas. Sci. Technol. 24 (2013) 1–8.
[9] H.C. Wang, I. Fedchenia, S.L. Shishkin, A. Finn, L.L. Smith, M. Colket, Sparsity-inspired image reconstruction for electrical capacitance tomography, Flow Meas. Instrum. 43 (2015) 59–71.
[10] J.M. Ye, H.G. Wang, W.Q. Yang, Image reconstruction for electrical capacitance tomography based on sparse representation, IEEE Trans. Instrum. Meas. 64 (2015) 89–102.
[11] E.A. Hosani, M. Zhang, J. Abascal, M. Soleimani, Imaging metallic samples using electrical capacitance tomography: forward modelling and reconstruction algorithms, Meas. Sci. Technol. 27 (2016) 1–11.
[12] M.A.R. Frias, W.Q. Yang, Real-time model-based image reconstruction with a prior calculated database for electrical capacitance tomography, Meas. Sci. Technol. 28 (2017) 1–14.
[13] E.A. Hosani, M. Soleimani, Multi-phase permittivity imaging using absolute value electrical capacitance tomography data and a level set algorithm, Proc. R. Soc. A 374 (2017) 1–18.
[14] C. Xia, C. Su, J. Cao, P. Li, Reconstruction of electrical capacitance tomography images based on fast linearized alternating direction method of multipliers for two-phase flow system, Chin. J. Chem. Eng. 24 (2016) 597–605.
[15] P. Wang, J.S. Lin, M. Wang, An image reconstruction algorithm for electrical capacitance tomography based on simulated annealing particle swarm optimization, J. Appl. Res. Technol. 13 (2015) 197–204.
[16] L.F. Zhang, Y.J. Zhai, X.G. Wang, P. Tian, Reconstruction method of electrical capacitance tomography based on wavelet fusion, Measurement 126 (2018) 223–230.
[17] M. Soleimani, W.R.B. Lionheart, Nonlinear image reconstruction for electrical capacitance tomography using experimental data, Meas. Sci. Technol. 16 (2005) 1987–1996.
[18] H.X. Wang, Electrical Tomography, Science Press, Beijing, 2013.
[19] J. Chen, M. Zhang, Y. Liu, J. Chen, Y. Li, Image reconstruction algorithms for electrical capacitance tomography based on ROF model using new numerical techniques, Meas. Sci. Technol. 28 (2017) 1–11.
[20] J. Lei, W.Y. Liu, Q.B. Liu, X.Y. Wang, S. Liu, Robust dynamic inversion algorithm for the visualization in electrical capacitance tomography, Measurement 50 (2014) 305–318.
[21] J. Lei, W.Y. Liu, S. Liu, X.Y. Wang, Dynamic imaging method using the low n-rank tensor for electrical capacitance tomography, Flow Meas. Instrum. 41 (2015) 104–114.
[22] C. Gunes, D.O. Acero, Q.M. Marashdeh, F.L. Teixeira, Acceleration of electrical capacitance volume tomography imaging by Fourier-based sparse representations, IEEE Sens. J. 18 (2018) 9649–9659.
[23] Z. Cao. L. Ji, L.J. Xu, Iterative reconstruction algorithm for electrical capacitance tomography based on Calderon's method, IEEE Sens. J. 18 (2018) 8450–8462.
[24] P. Chu, J. Lei, Q.B. Liu, Prior image induced regularization method for electrical capacitance tomography, IEEE Access 7 (2018) 2490–2501.
[25] G. Guo, G.W. Tong, L. Lu, S. Liu, Iterative reconstruction algorithm for the inverse problems in electrical capacitance tomography, Flow Meas. Instrum. 64 (2018) 204–212.
[26] G.W. Tong, S. Liu, H.Y. Chen, X.Y. Wang, Regularization iteration imaging algorithm for electrical capacitance tomography, Meas. Sci. Technol. 29 (3) (2018) http://dx.doi.org/10.1088/1361-6501/aaa3c5.
[27] H. Wang, H.L. Hu, L.J. Wang, H.X. Wang, Image reconstruction for an electrical capacitance tomography (ECT) system based on a least squares support vector machine and bacterial colony chemotaxis algorithm, Flow Meas. Instrum. 27 (2012) 59–66.
[28] J. Lei, S. Liu, X.Y. Wang, Q.B. Liu, An image reconstruction algorithm for electrical capacitance tomography based on robust principle component analysis, Sensors 13 (2) (2013) 2076–2092.
[29] W.Q. Yang, L.H. Peng, Image reconstruction algorithms for electrical capacitance tomography, Meas. Sci. Technol. 14 (2003) R1–R13.
[30] T. Goldstein, S. Osher, The split Bregman method for L1-regularized problems, SIAM J. Imaging Sci. 2 (2009) 323–343.
[31] S. Boyd, N. Parikh, E. Chu, B. Peleato, J. Eckstein, Distributed optimization and statistical learning via the alternating direction method of multipliers, Found. Trends Mach. Learn. 3 (2011) 1–122.
[32] B. Liu, Y.M. Li, Z.L. Xu, Manifold regularized matrix completion for multi-label learning with ADMM, Neural Netw. 101 (2018) 57–67.
[33] C. Lu, J. Feng, S. Yan, Z. Lin, A unified alternating direction method of multipliers by majorization minimization, IEEE Trans. Pattern Anal. Mach. Intell. 40 (2018) 527–541.
[34] P.L. Combettes, V.R. Wajs, Signal recovery by proximal forward-backward splitting, Multiscale Model. Simul. 4 (2005) 1168–1200.
[35] B.B. Hao, J.G. Zhu, Fast L1 regularized iterative forward backward splitting with adaptive parameter selection for image restoration, J. Vis. Commun. Image Represent. 44 (2017) 139–147.
[36] Q.Z. Lin, B.S. Hu, Y. Tang, L.Y. Zhang, J.Y. Chen, X.M. Wang, Z. Ming, A local search enhanced differential evolutionary algorithm for sparse recovery, Appl. Soft Comput. 57 (2017) 144–163.
[37] Y.M. Li, D. Wei, Delayed Lagrange neural network for sparse signal reconstruction under compressive sampling, Optik 127 (2016) 7077–7082.
[38] L. Vidya, V. Vivekanand, U. Shyamkumar, M. Deepak, RBF-network based sparse signal recovery algorithm for compressed sensing reconstruction, Neural Netw. 63 (2015) 66–78.
[39] A. Beck, M. Teboulle, A fast iterative shrinkage-thresholding algorithm for linear inverse problems, SIAM J. Imaging Sci. 2 (2009) 183–202.
[40] Y.C. Yu, J.G. Peng, X.L. Han, A.G. Cui, A primal Douglas-Rachford splitting method for the constrained minimization problem in compressive sensing, Circuits Systems Signal Process. 36 (2017) 4022–4049.
[41] D.A. Lorenz, S. Wenger, F. Schöpfer, M. Magnor, A sparse Kaczmarz solver and a linearized Bregman method for online compressed sensing, in: IEEE International Conference on Image Processing (ICIP), 2014, pp. 1347–1351.
[42] F. Schöpfer, D.A. Lorenz, Linear convergence of the randomized sparse Kaczmarz method, Math. Program. 1-2 (2019) 509–536.
[43] S. Yun, K.C. Toh, A coordinate gradient descent method for L1-regularized convex minimization, Comput. Optim. Appl. 48 (2011) 273–307.
[44] J. Prakash, D. Sanny, S.K. Kalva, M. Pramanik, P.K. Yalavarthy, Fractional regularization to improve photoacoustic tomographic image reconstruction, IEEE Trans. Med. Imaging (2018) http://dx.doi.org/10.1109/tmi.2018.2889314.
[45] S. Morigi, L. Reichel, F. Sgallari, Fractional Tikhonov regularization with a nonlinear penalty term, J. Comput. Appl. Math. 324 (2017) 142–154.
[46] N. Lynn, P.N. Suganthan, Ensemble particle swarm optimizer, Appl. Soft Comput. 55 (2017) 533–548.
[47] B. Ma, Y. Xia, A tribe competition-based genetic algorithm for feature selection in pattern classification, Appl. Soft Comput. 58 (2017) 328–338.
[48] M. Alswaitti, M. Albughdadi, N.A.M. Isa, Variance-based differential evolution algorithm with an optional crossover for data clustering, Appl. Soft Comput. 80 (2019) 1–17.
[49] T. Dokeroglu, E. Sevinc, A. Cosar, Artificial bee colony optimization for the quadratic assignment problem, Appl. Soft Comput. 76 (2019) 595–606.
[50] Q. Tu, X. Chen, X. Liu, Multi-strategy ensemble grey wolf optimizer and its application to feature selection, Appl. Soft Comput. 76 (2019) 16–30.
[51] X. Zhang, M. Burger, X. Bresson, S. Osher, Bregmanized nonlocal regularization for deconvolution and sparse reconstruction, SIAM J. Imaging Sci. 3 (2010) 253–276.
[52] J. Duchi, Y. Singer, Efficient online and batch learning using forward backward splitting, J. Mach. Learn. Res. 10 (2009) 2899–2934.
[53] L.B. Montefusco, D. Lazzaro, S. Papi, C. Guerrini, A fast compressed sensing approach to 3D MR image reconstruction, IEEE Trans. Med. Imaging 30 (2011) 1064–1075.
[54] J.A.K. Suykens, T. Van Gestel, J. De Brabanter, B. De Moor, J. Vandewalle, Least Squares Support Vector Machines, World Scientific, Singapore, 2002.
[55] Y. Lv, F. Hong, T.T. Yang, F. Fang, J.Z. Liu, A dynamic model for the bed temperature prediction of circulating fluidized bed boilers based on least squares support vector machine with real operational data, Energy 124 (2017) 284–294.
[56] S. Dasgupta, Experiments with random projection, in: Proceedings of the Sixteenth Conference on Uncertainty in Artificial Intelligence, Morgan Kaufmann Publishers Inc., San Francisco, CA, USA, 2000, pp. 143–151.

[57] H.Z. Xie, J. Li, Q.S. Zhang, Y.D. Wang, Comparison among dimensionality reduction techniques based on random projection for cancer classification, Comput. Biol. Chem. 65 (2016) 165–172.
[58] E. Bingham, H. Mannila, Random projection in dimensionality reduction: Applications to image and text data, in: International Conference on Knowledge Discovery and Data Mining, 2001, pp. 245–250.
[59] O. Sagi, L. Rokach, Ensemble learning: A survey, Data Min. Knowl. Discov. 8 (2018) 1–18.
[60] J. Mendes-Moreira, C. Soares, A.M. Jorge, J.F. de Sousa, Ensemble approaches for regression: A survey, ACM Comput. Surv. 45 (2012) 1–10.
[61] R. Storn, K. Price, Differential evolution-a simple and efficient heuristic for global optimization over continuous spaces, J. Global Optim. 11 (1997) 341–359.
[62] K. Price, R.M. Storn, J.A. Lampinen, Differential Evolution: A Practical Approach to Global Optimization, Springer, 2005.
[63] S. Das, S.S. Mullick, P.N. Suganthan, Recent advances in differential evolution-an updated survey, Swarm Evol. Comput. 27 (2016) 1–30.
[64] R.D. Al-Dabbagh, F. Neri, N. Idris, M.S. Baba, Algorithmic design issues in adaptive differential evolution schemes: Review and taxonomy, Swarm Evol. Comput. 43 (2018) 284–311.
[65] L.Z. Cui, C. Xu, G.H. Li, Z. Ming, Y.H. Feng, N. Lu, A high accurate localization algorithm with DV-hop and differential evolution for wireless sensor network, Appl. Soft Comput. 68 (2018) 39–52.
[66] A. Khan, C. Niemann-Delius, A differential evolution based approach for the production scheduling of open pit mines with or without the condition of grade uncertainty, Appl. Soft Comput. 66 (2018) 428–437.
[67] P.P. Biswas, P.N. Suganthan, G.A.J. Amaratunga, Minimizing harmonic distortion in power system with optimal design of hybrid active power filter using differential evolution, Appl. Soft Comput. 61 (2017) 486–496.